EFFECTS OF CANYON TOPOGRAPHY ON STRONG GROUND MOTION

BY H. L. WONG AND P. C. JENNINGS

ABSTRACT

The two-dimensional scattering and diffraction of *SH* waves of arbitrary angle of incidence from irregular, canyon-shaped topography is formulated in terms of an integral equation. Taking advantage of the simple boundary conditions of *SH*-wave problems, the method of images is applied to reduce the integral equation to one with a finite integral, which can readily be solved numerically by available methods.

The method is first applied to the analytically solved case of a cylindrical canyon to verify its accuracy, and then to two idealized cross sections based upon Pacoima Canyon to investigate the effects of topography in a more realistic case. The results of the harmonic analysis include wave amplification patterns and transfer functions for different wavelengths and for different angles of incidence. The study also includes analysis of transient motions. With the N76°W component of the Pacoima Dam accelerogram specified to occur at one point in the cross section, the effects of different angles of incidence upon the required input motion and upon the motion at several other points in the cross section were examined by calculating accelerograms and response spectra.

The effects of canyon-shaped topography are seen most prominently in the amplification patterns and transfer functions for harmonic response, wherein shielding and focusing can cause variations up to a factor of six for wavelengths comparable to, or shorter than, the canyon width. In the case of transient motions, the accelerograms at different points show significant differences, but not as large as seen in the harmonic analysis. The response spectra show the smallest differences; significant effects are confined to the higher frequencies.

INTRODUCTION

A detailed understanding of the effects of topographic features upon strong ground motion would be of obvious value to earthquake engineering and seismology, but it has not yet been achieved because of the scarcity of measured shaking and the difficulties in obtaining theoretical solutions to realistic problems. In recent years, however, significant progress has been made in the development of solutions to some simple problems. One of the most extensive studies of topographic effects on strong ground motion is that done by Riemer *et al.* (1974). In that study, a three-dimensional, finite element method was used to model Pacoima Canyon and Pacoima Dam in an effort to examine, under simplified conditions of wave propagation, the effects of topography and dam-foundation interaction upon the strong motion accelerogram recorded near one abutment during the San Fernando earthquake. Most other studies of topographic effects have been two-dimensional (e.g., Boore, 1972, 1973; Bouchon, 1973; Trifunac, 1973; Asano, 1966; McIvor, 1969; Wong and Trifunac, 1974). The studies by Boore (1972, 1973) use finite differences to consider transient motions; the other studies cited determined steady-state response to harmonic excitation. Bouchon (1973) used the method developed by Aki and Larner (1970) to estimate the effects of irregular surfaces under the condition of shallow slopes and incident motion with long wavelengths. Studies of

individual, simplified geometries were accomplished by McIvor (1969), by Boore (1973), and by Asano (1966), who studied a corrugated surface and by Trifunac (1973) and Wong and Trifunac (1974). The latter two studies treat scattering and diffraction of *SH* waves by cylindrical and elliptical discontinuities, respectively, using separation of variables.

The purpose of the present study is to introduce a method for calculating the two-dimensional scattering of incident *SH* motions by an arbitrarily-shaped canyon. As shown schematically in Figure 1, the method uses images to satisfy the boundary conditions on the surface of the half-space away from the portion of arbitrary surface. The accuracy of the approach is illustrated first by comparing the results with the exact solution for a cylindrical canyon. The method is then applied to two idealized cross
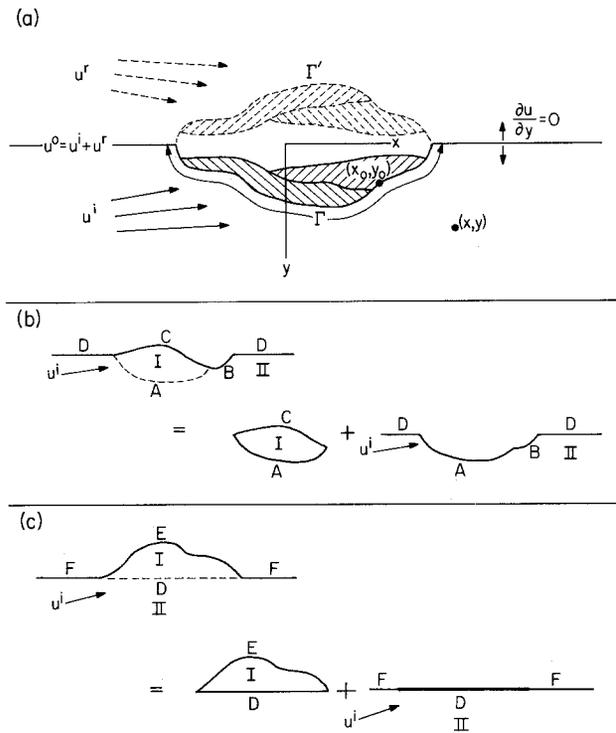

FIG. 1. (a) The symmetrical formulation of the image problem. (b) The method of images applied to elevated topographies. (c) Alternative approach for topographies totally above the half-space.

sections taken from Pacoima Canyon to obtain additional insight into effects of topography on strong ground motion. Both steady-state harmonic response and transient response, using the N75°W component of the Pacoima Dam accelerogram, are included in the analysis.

METHOD OF ANALYSIS

If only two-dimensional *SH*-waves are considered, the anti-plane displacement, u, satisfies the scalar-wave equation

$$\frac{\partial^2 u}{\partial x^2} + \frac{\partial^2 u}{\partial y^2} = \frac{1}{\beta^2} \frac{\partial^2 u}{\partial t^2} \tag{1}$$

where $\beta = (\mu/\rho)^{1/2}$ is the velocity of shear-wave propagation, μ is the shear modulus, and ρ is the density of the medium. For harmonic waves of the form $u \exp(i\omega t)$, the time dependence of (1) may be separated, leaving the Helmholtz equation

$$\frac{\partial^2 u}{\partial x^2} + \frac{\partial^2 u}{\partial y^2} + \kappa^2 u = 0 \qquad (\kappa = \omega/\beta). \quad (2)$$

The Green's function $G^*(\mathbf{r} \mid \mathbf{r}_0)$ of equation (2) for outgoing waves in an infinite full-space is the Hankel function of the second kind and zeroth order (Morse and Feshbach, 1953)

$$G^*(\mathbf{r} \mid \mathbf{r}_0) = (i/4) H_0^{(2)}(\kappa|\mathbf{r} - \mathbf{r}_0|) \quad (3)$$

which satisfies the equation

$$\left(\frac{\partial^2}{\partial x^2} + \frac{\partial^2}{\partial y^2} + \kappa^2 \right) G^*(\mathbf{r} \mid \mathbf{r}_0) = -\delta(\mathbf{r} - \mathbf{r}_0) \quad (4)$$

where $\mathbf{r} = \mathbf{r}(x, y)$ and $\mathbf{r}_0 = \mathbf{r}(x_0, y_0)$ are the position vectors of the observation point and source point, respectively.

In analytical studies of local effects on surface motions, the basic geometrical configuration is the half-space. Due to the simple boundary conditions involved in the SH-wave problem considered here, the method of images can be applied to determine the Green's function for a point in a half-space. The symmetry about the x-axis (Figure 1a) produces the required condition of zero stresses, $\mu(\partial u/\partial y) = 0$ at the plane surface on either side of the surface Γ, the irregular interface to be studied. The boundary conditions on Γ require continuous displacements and stresses across the interface.

The Green's function for a point in a half-space is found from superposition of the Green's functions for the full-space for the point of interest and its image point.

$$G(x, y \mid x_0, y_0) = i/4[H_0^{(2)}(\kappa[(x - x_0)^2 + (y - y_0)^2]^{1/2})$$
$$+ H_0^{(2)}(\kappa[(x - x_0)^2 + (y + y_0)^2]^{1/2})]. \quad (5)$$

Using $G(\mathbf{r} \mid \mathbf{r}_0)$, Weber's integral formula for determination of the values of u and $\partial u/\partial n_0$ (n_0 is the unit normal at $\mathbf{r}_0$ on Γ) at the interface Γ is

$$\frac{1}{2} u(\mathbf{r}) - \int_\Gamma \left[u(\mathbf{r}_0) \frac{\partial G(\mathbf{r} \mid \mathbf{r}_0)}{\partial n_0} - G(\mathbf{r} \mid \mathbf{r}_0) \frac{\partial u(\mathbf{r}_0)}{\partial n_0} \right] ds_0 = u^0(\mathbf{r}), \ \mathbf{r} \text{ on } \Gamma \quad (6)$$

where $u^0(\mathbf{r})$ is the total wave field for a half-space with the irregular surface Γ absent. It is noted from equation (6) that the method of images has made it possible to obtain a finite integral equation, a feature which has computational advantages. It should be noted also that the boundary values at the irregular surface, $u(\mathbf{r}_0)$ and $\partial u(\mathbf{r}_0)/\partial n_0$ in equation (6), are not necessarily independent of each other. The displacement $u(\mathbf{r})$ outside of the boundary Γ is related to the boundary values by

$$u(\mathbf{r}) = u^0(\mathbf{r}) - \int_\Gamma \left[u(\mathbf{r}_0) \frac{\partial G(\mathbf{r} \mid \mathbf{r}_0)}{\partial n} - G(\mathbf{r} \mid \mathbf{r}_0) \frac{\partial u(\mathbf{r}_0)}{\partial n_0} \right] ds_0. \quad (7)$$

A detailed derivation of equations (6) and (7) may be found in Mow and Pao (1971).

Although only concave topography is considered here, the method can be extended to study convex topography as illustrated schematically in Figure 1, b and c. In this case the problem is first separated into an exterior problem II and an interior problem I, Figure 1b. The exterior problem II has a concave geometry and the method of images can again be applied as outlined above. The conditions at each of the surfaces B, C, and D are

stress-free requirements; while at surface A, the corresponding displacements and stresses must be equated for I and II, a continuity requirement. Therefore, the two problems are solved with coupled boundary conditions. Another case of interest is illustrated in Figure 1c in which the surface topography is totally above the half-space. For this case, surfaces E and F are stress-free and the continuity conditions for displacements and stresses are required for surface D. Problem II now consists of a half-space with line sources along the surface D while the interior problem I is analyzed by the method of images.

NUMERICAL APPROXIMATION

The integral equation, (6) can be solved in closed form only when $G(\mathbf{r} \mid \mathbf{r}_0)$ can be expanded into a series of orthogonal eigenfunctions, an approach suitable for only a few simple geometries. For irregularly shaped boundaries, equation (6) may be solved numerically by replacing the integral by a finite sum, and finding the unknown values of $u(r_0)$ and $\partial u(\mathbf{r}_0)/\partial n_0$ at N discrete locations on the surface. The imaginary part of the kernel $G(\mathbf{r} \mid \mathbf{r}_0)$ is singular at $\mathbf{r} = \mathbf{r}_0$, however, so to avoid numerical problems, a mathematical limit must be taken for this portion of the integration. The other parts of the integral can be treated directly. After the boundary values $u(\mathbf{r}_0)$ and $\partial u(\mathbf{r}_0)/\partial n_0$ are calculated, the values of $u(\mathbf{r}_0)$ at other points can be obtained from equation (7).

Details of the method of calculation and its limitations as discussed by Banaugh and Goldsmith (1963a and b) apply here, even though their Green's function is slightly different. The programming of the problem is much simpler in the present application, however, because modern computer software allows direct arithmetical operations with complex numbers; the real and imaginary parts need not be considered separately. One of the advantages of the method is its relatively rapid convergence. The errors are of order $h^2 \log h$, where h is the distance between the N equally spaced points (de Hoog and Weiss, 1973).

For application to canyon topography, the stress is zero on the surface Γ as well as on the planar surface on either side. Hence, $\partial u(\mathbf{r}_0)/\partial n_0 = 0$ and equation (6) is simplified to

$$\frac{1}{2} u(\mathbf{r}) - \int_\Gamma u(\mathbf{r}_0) \frac{\partial G(\mathbf{r}_0 \mid \mathbf{r})}{\partial n_0} ds_0 = u^0(\mathbf{r}), \mathbf{r} \text{ on } \Gamma. \tag{8}$$

The wave field $u^0(\mathbf{r})$ can be a superposition of SH waves from arbitrary sources plus their reflections from the boundary of the half-space, but for purposes of illustrating the effects of canyon topography upon ground motion, and for simplicity, only plane incident SH-waves were assumed.

An incident harmonic plane wave of unit magnitude, making a counterclockwise angle θ with respect to the x axis has the representation

$$u^i(\mathbf{r}) = \exp\left[(i\omega/\beta)(-x \cos\theta + y \sin\theta)\right] \tag{9}$$

in which the factor exp $(i\omega t)$ is understood. To obtain $u^0(\mathbf{r})$ it is necessary to add to $u^i(\mathbf{r})$ a reflected wave, $u^r(\mathbf{r})$, with an angle of $-\theta$. Thus

$$u^0(\mathbf{r}) = u^i(\mathbf{r}) + u^r(\mathbf{r}) = 2 \exp\left[-(i\omega x/\beta) \cos\theta\right] \cos\left[(\omega y/\beta) \sin\theta\right]. \tag{10}$$

With $u^0(\mathbf{r})$ specified, equation (8) becomes a Fredholm integral equation of the second kind for the unknown function $u(\mathbf{r})$, $\mathbf{r}$ on Γ. By first parameterizing x and y as functions of ξ

$$x = x(\xi), y = y(\xi); 0 \leqq \xi \leqq \pi \tag{11}$$

the finite integral in equation (8) may be changed to an integral on the dummy variable ξ. In the integration ds_0 is replaced by

$$ds_0 = \left[\left(\frac{dx}{d\xi}\right)^2 + \left(\frac{dy}{\partial\xi}\right)^2\right]^{1/2} d\xi. \tag{12}$$

Calculating the integral as if $u(\mathbf{r}_0)$ is known, by using the trapezoidal rule, the continuous integral of equation (8) discretizes into N simultaneous equations.

$$\left[\frac{1}{2} + \frac{1}{4(N-1)}\left(\frac{x_\xi y_{\xi\xi} - y_\xi x_{\xi\xi}}{x_\xi^2 + y_\xi^2}\right)\right]u(x_l, y_l)$$

$$- \frac{2\kappa\pi}{(N-1)}\sum_{\substack{j=1 \\ j\neq l}}^{N}\frac{\partial G}{\partial n_0}(x_j, y_j \mid x_l, y_l)\left[\frac{(x_j-x_l)y_\xi - (y_i-y_l)x_\xi}{[(x_j-x_l)^2+(y_j-y_l)^2]^{1/2}}\right]u(x_j, y_j) = u^0(x_l, y_l)$$

$$l = 1, 2, 3, \ldots, N \tag{13}$$

in which $G(x_j, y_j \mid x_l, y_l)$ is as defined in equation (5), and N is the number of discrete points on the boundary Γ. Equation (13) for the unknowns $u(x_l, y_l)$ has the form of a standard problem in linear algebra

$$[A_{lj}]\{u(x_j, y_j)\} = \{u^0(x_l, y_l)\} \tag{14}$$

in which the elements of (A_{lj}) are constants, and is therefore in a form convenient for numerical computations.

To investigate the accuracy of the calculation method, the solution of equation (13) was compared to the exact solution for scattering by a circular canyon with radius a. Letting $x = a\cos\xi$ and $y = a\sin\xi$, the surface Γ becomes a semi-circular cylinder, the configuration studied by Trifunac (1973). To obtain a direct comparison of the values of u on the surface Γ, the dimensionless frequency η is again used here

$$\eta = 2a/\lambda = \omega a/\pi\beta. \tag{15}$$

The variable η is the ratio of the width of the canyon to the incident wavelength; large values indicate waves with lengths short compared to the width of the canyon.

Table 1 gives values of the real and imaginary parts of u on Γ for $\eta = 0.5, 2.0$ and for angles of incidence of $0°$ and $60°$. Three sets of solutions calculated for different values of N are listed to indicate the rate of convergence. Note that for low frequencies, even $N = 4$ yields answers of acceptable accuracy, although more points are clearly needed for higher frequencies.

APPLICATION TO CANYON TOPOGRAPHY

Attention is next turned to more realistic shapes in order to study the effects of topography upon strong ground motion. Two idealized cross sections based on the topography of Pacoima Canyon were selected for study. As shown in Figure 2a (Trifunac, 1973), the topography is quite complex, but in the vicinity of the dam it might be permissible to idealize the site as two-dimensional for the purposes of studying motion in the longitudinal (N76°W) direction. This assumption will be examined later in the light of the numerical results. The idealized cross sections used in the analysis (Figures 3 and 4) are taken from sections C and D of Figure 2a; section C includes the location of the accelerograph which recorded the motion during the San Fernando earthquake. Section D is 70 meters downstream from C.

TABLE 1

COMPARISON OF RESULTS TO EXACT SOLUTION FOR A SEMICYLINDRICAL CANYON

$\theta = 0°, \eta = 0.5$

	N = 4	N = 7	N = 25	Exact
x/a = 1.00	(-1.61626, 0.14186)	(-1.58401, 0.20458)	(-1.57965, 0.20761)	(-1.57964, 0.20760)
x/a = 0.50	(1.31137, 1.21450)	(1.32828, 1.15243)	(1.32786, 1.14952)	(1.32787, 1.14951)
x/a = -0.50	(1.87391, -2.59291)	(1.80520, -2.52326)	(1.80365, -2.52046)	(1.80366, -2.52048)
x/a = -1.00	(-0.87818, -3.49553)	(-0.78959, -3.52299)	(-0.78661, -3.51834)	(-0.78662, -3.51835)

$\theta = 60°, \eta = 2.0$

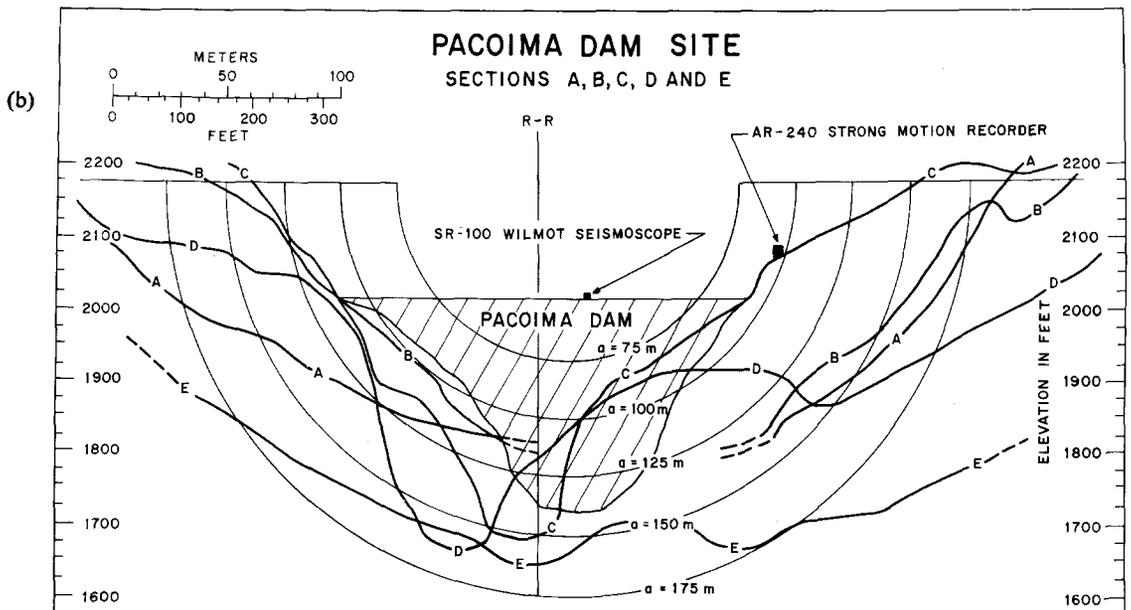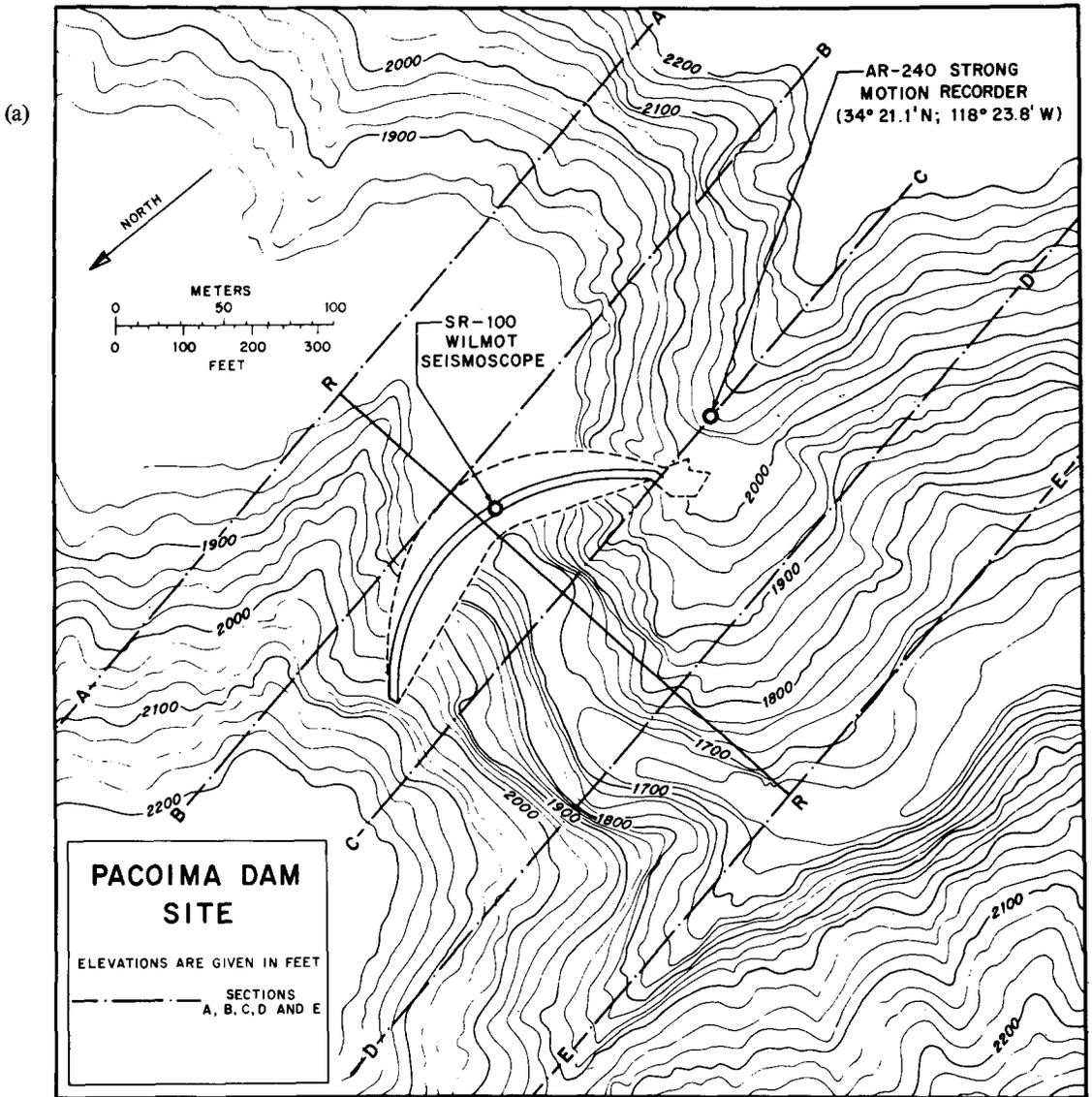|	N = 13	N = 25	N = 49	Exact
x/a = 1.00	(-1.43294, -0.76424)	(-1.42491, -0.72856)	(-1.42419, -0.72513)	(-1.42406, -0.72470)
x/a = 0.50	(-1.76236, -0.17628)	(-1.76342, -0.20332)	(-1.76343, -0.20625)	(-1.76346, -0.20662)
x/a = -0.50	(1.24621, -0.53489)	(1.25058, -0.50135)	(1.25087, -0.49797)	(1.25095, -0.49755)
x/a = -1.00	(-3.48503, 0.45972)	(-3.47883, 0.43055)	(-3.47835, 0.42753)	(-3.47833, 0.42714)

FIG. 2. (a) Pacoima Canyon in the vicinity of Pacoima Dam. (b) Cross sections of Pacoima Canyon (Trifunac, 1973).

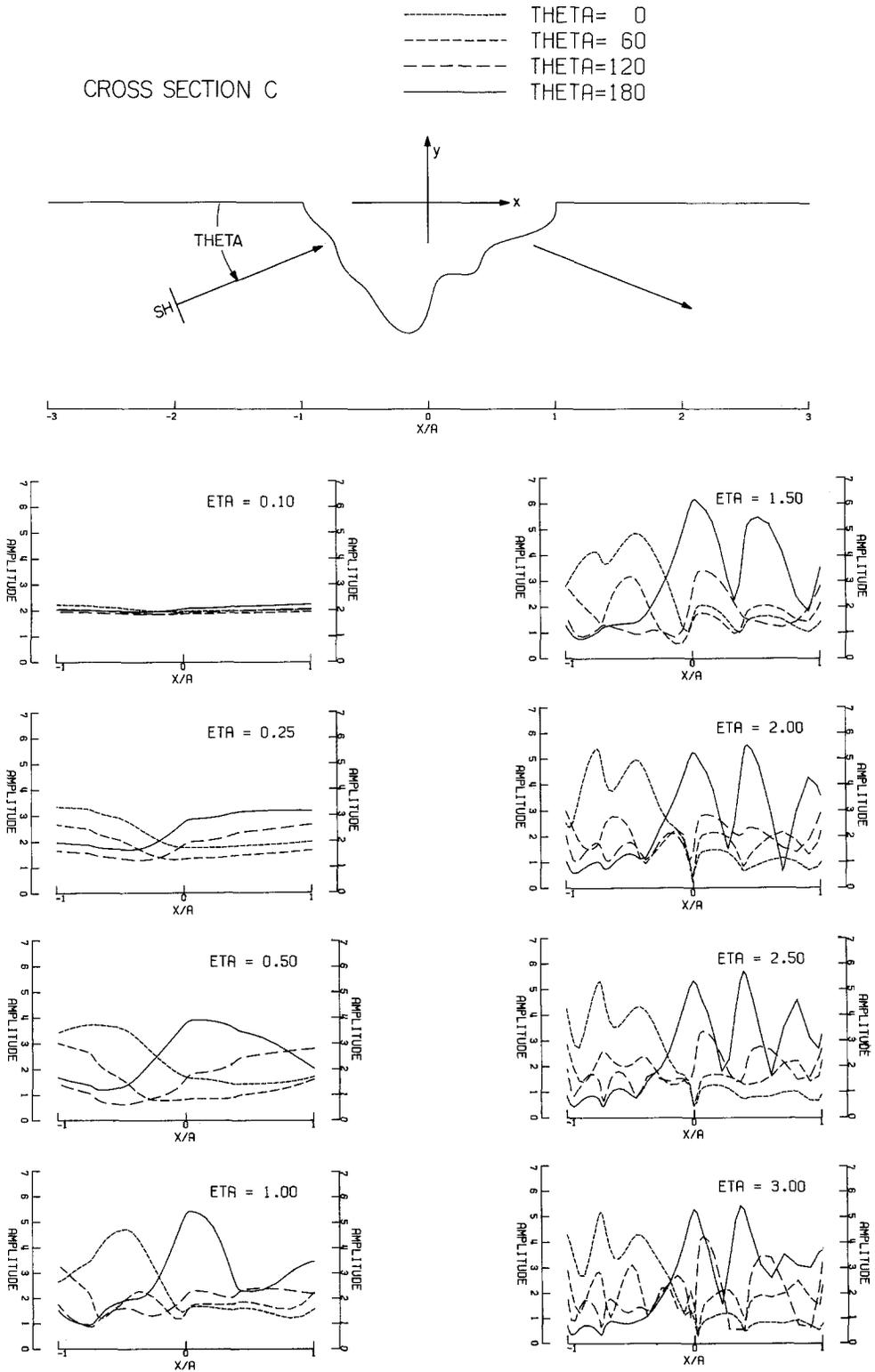FIG. 3. Displacement amplitudes along the surface of cross-section C due to unit incident waves with angles of incidence, $\theta = 0°$, $60°$, $120°$, $180°$.
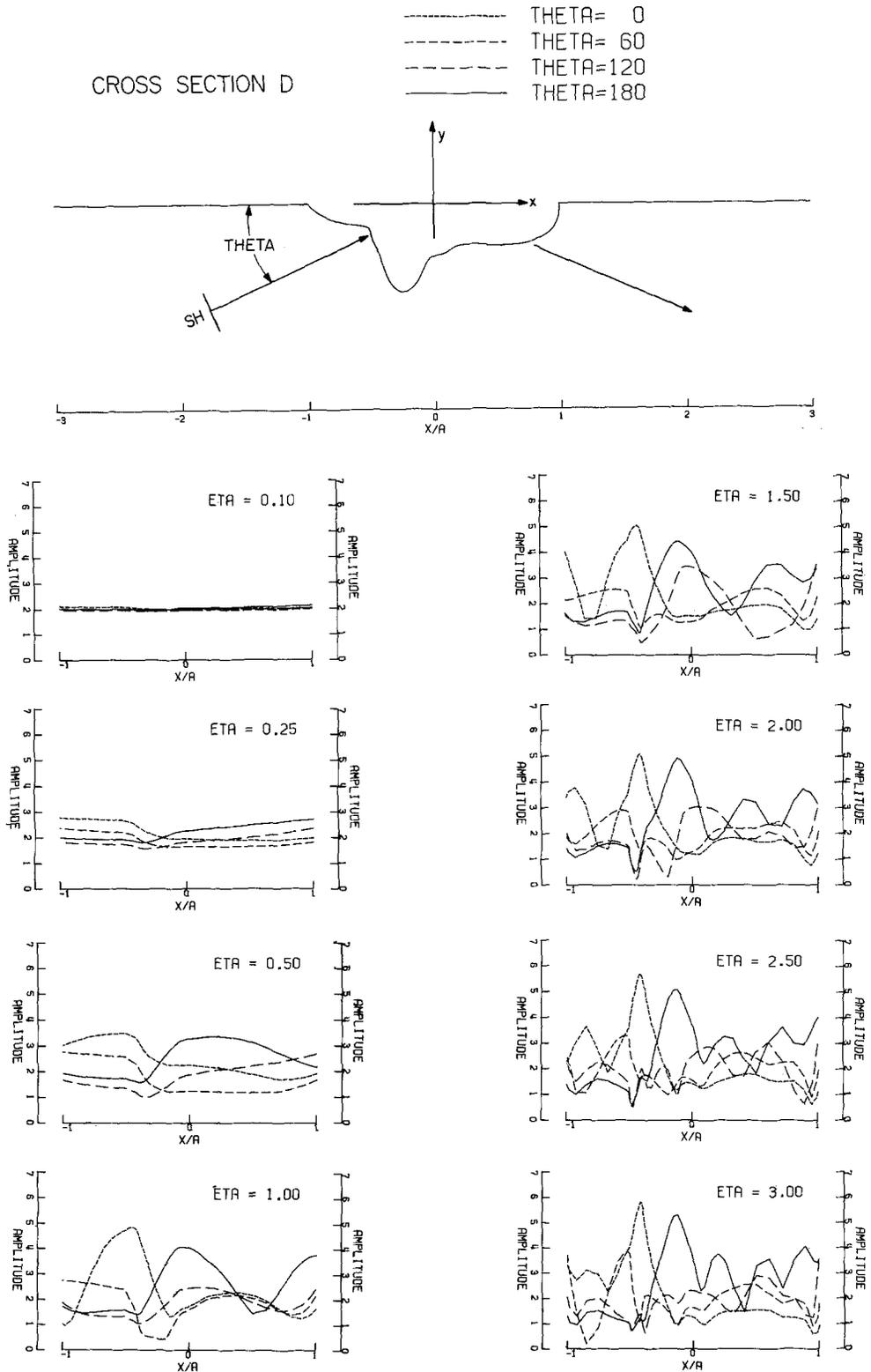
FIG. 4. Displacement amplitudes along the surface of cross-section D due to unit incident waves with angles of incidence, $\theta = 0°, 60°, 120°, 180°$.

The idealized cross sections were constructed by fitting approximately the coordinates of sections C and D of Figure 2 by ten terms of a Fourier series in ξ. This expresses the boundary in a form similar to the last example and subsequent steps in the analysis follow those for the circular case. A shear-wave velocity of 2.5 km/sec was chosen for the calculations. The results obtained for the two cross sections are given in Figures 3 and 4 which show the amplitude of steady-state displacement due to a harmonic incident wave of unit amplitude plotted against the dimensionless projected distance x/a. Plots are given for eight values of the dimensionless frequencies η. The half-width of the canyon is a, chosen for convenience of comparison with the results for a cylindrical canyon. On these plots a half-space without the canyon would show an amplitude of two, the sum of the incident and reflected waves. Since the shape of the canyon is irregular and is non-symmetric, the angle of incidence is expected to play an important role in the diffraction pattern, therefore, four angles of incidence $\theta = 0°$, $60°$, $120°$, and $180°$ were considered. The case when $\theta = 0°$ corresponds to an incident wave traveling from left to right.

Figures 3 and 4 show that the overall trends of amplification and reduction are dependent on the angle of incidence, the dimensionless frequency, and the geometrical shape. The topographic effects are, of course, much more prominent when the wavelength of the incident motion is comparable to, or less than, the dimensions of the canyon, i.e., when η is large. The amplitude varies rapidly from point to point for these short wavelengths, and at some locations, amplitudes six times the input occur. At other points the motion is almost zero. The large amplifications and reductions are consequences of focusing and shielding; this occurs most prominently for horizontally incident waves. It has been indicated (Wong and Trifunac, 1974) that the maximum amplification of the input for an elliptical canyon does not exceed four, the amplification shown by a quarter-space. In the present case, the amplifications significantly greater than four occur at the interior convexities of the cross sections. It is the quasi-resonant behavior of these local convexities at certain frequencies that lead to the high amplifications. Bouchon (1973) and Boore (1973) also have pointed out that convex topographic features usually yield larger amplifications than concave topography. The locations where the amplitudes are nearly zero are similar to the nodes of a standing-wave pattern. Although the translational motions at these points are quite small, the motions at some of these points have a torsional character as a result of a rapid local change of phase (Trifunac, 1973). Of course, these results are for steady-state harmonic response at a few selected frequencies only, and generalizations to other situations must be made cautiously.

As the wavelengths become long compared to the dimensions of the canyon, the details of the topography no longer influence the results. This can be seen in plots for $\eta = 0.25$ and $\eta = 0.10$ in Figures 3 and 4 (2.5 and 1.0 Hz, respectively, for $\beta = 2.5$ km/sec and $a = 0.12$ km) which show the amplification to approach two, the value for a featureless half-space. Also, the variation across the canyon is not large for various angles of incidence. Therefore, focusing and shielding are not significant for these conditions for frequencies of about 1.0 Hz or less.

Some insight into the adequacy of the two-dimensional idealization of canyon topography may be gained from comparing Figures 3 and 4. For $\eta = 0.5$ or less (frequencies less than 5 Hz) the plots are quite similar, and there is some similarity for $\eta = 1.00$ (10 Hz). For higher values of η, however, the locations of the peaks differ greatly. Since the difference in the amplification patterns of the two neighboring cross sections is one measure of the three-dimensional nature of the effects of topography on the motion, the different locations of major peaks indicate that the two-dimensional assumption is not appropriate for these values of β and a for frequencies higher than about 5 to 10 Hz.

TABLE 2

COMPARISON OF NUMERICAL RESULTS FOR TWO DIFFERENT GRID SPACINGS

x/a	θ = 60°		θ = 120°	
	N = 37	N = 49	N = 37	N = 49
			$\eta = 0.50$	
1.000	(1.21480, 1.03881)	(1.21456, 1.03868)	(1.55384, -2.31533)	(1.55357, -2.31486)
0.034	(0.53664, -0.63355)	(0.53687, -0.63378)	(0.83768, -1.58088)	(0.83810, -1.58152)
-0.230	(0.18305, -0.76240)	(0.18304, -0.76226)	(0.04775, -0.88614)	(0.04778, -0.88599)
-0.511	(1.13487, -1.17440)	(1.13489, -1.17449)	(0.47683, -0.39398)	(0.47677, -0.39398)
-1.000	(2.19941, -2.04638)	(2.19926, -2.04630)	(1.22012, 0.74974)	(1.21998, 0.74965)
			$\eta = 2.00$	
1.000	(-1.60306, -1.47831)	(-1.60392, -1.46677)	(-1.83523, 2.25714)	(-1.83262, 2.24536)
0.034	(-0.49496, -1.61972)	(-0.50250, -1.60994)	(-1.15628, 2.24117)	(-1.15285, 2.25589)
-0.230	(1.51389, 0.96970)	(1.50820, 0.96395)	(1.82704, 0.80186)	(1.81946, 0.79875)
-0.511	(-0.46180, 2.33184)	(-0.46586, 2.34038)	(-1.73736, -0.34711)	(-1.73287, -0.34255)
-1.000	(-2.29348, -1.95721)	(-2.28971, -1.95356)	(-1.55588, 1.31090)	(-1.55226, 1.30796)

The results suggest that it is probably valid to use two-dimensional idealization to study effects at low frequencies, but that peak accelerations and other high-frequency phenomena must be analyzed by more sophisticated methods.

To investigate the rate of convergence of the solution for this topography, values of displacement at five locations and two frequencies are compared in Table 2 for $N = 37$ and $N = 49$. The maximum difference between corresponding numbers is 1.5 per cent for $\eta = 2.00$, indicating that the true error would be less than this amount, since the errors are of order $1/N^2 \log (1/N)$ (de Hoog and Weiss, 1973).
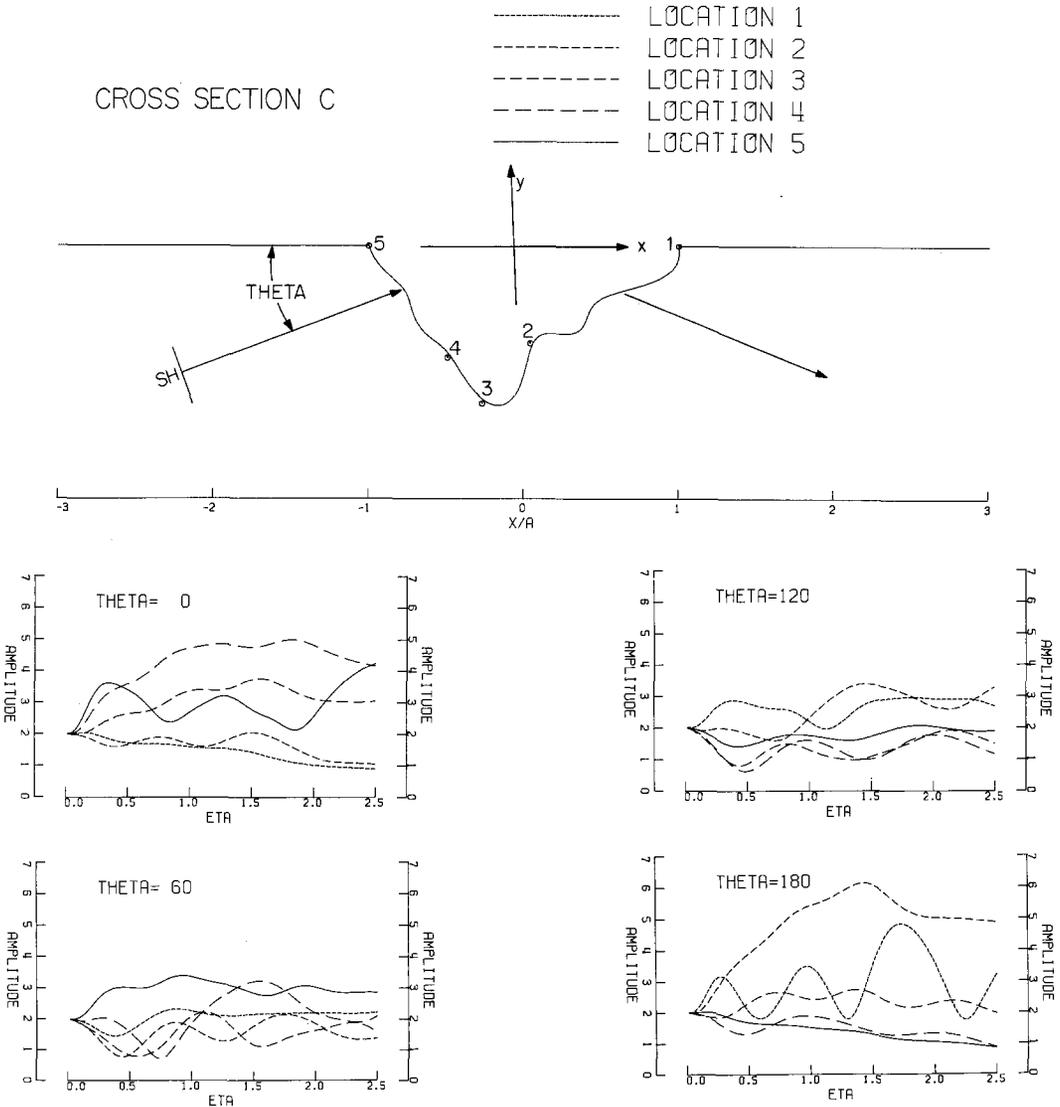

FIG. 5. Spectral amplification $T_{oj}(\eta)$ of five locations in cross-section C for angles of incidence, $\theta = 0°$, 60°, 120°, 180°.

EFFECTS ON TRANSIENT MOTIONS

The effects of the chosen topography upon transient motions can be studied by Fourier analysis and synthesis, using the solutions obtained in the frequency domain. If the

complex transfer function $T_{jk}(\omega)$ from point j to point k is known, the Fourier transform of the motion $Z_k(\omega)$, and hence the motion itself, at point k may be obtained from $Z_j(\omega)$, the Fourier transform of the motion at point j, i.e.,

$$Z_k(\omega) = T_{jk}(\omega)Z_j(\omega) \tag{16}$$

and

$$T_{jk}(\omega) = [T_{0k}(\omega)]/[T_{0j}(\omega)] \tag{17}$$

where $T_{0k}(\omega)$ and $T_{0j}(\omega)$ are the transfer functions from the incident motion $u^0(\mathbf{r})$ to locations k and j, respectively.

Equations (16) and (17) were applied by storing the transfer functions $T_{0j}(\eta)$ from a plane incident wave to five locations of canyon profile C, as shown in Figure 5. The moduli of the transfer functions, $|T_{0j}(\eta)|$, $j = 1, 2, \ldots, 5$ are shown in Figure 5 for four angles
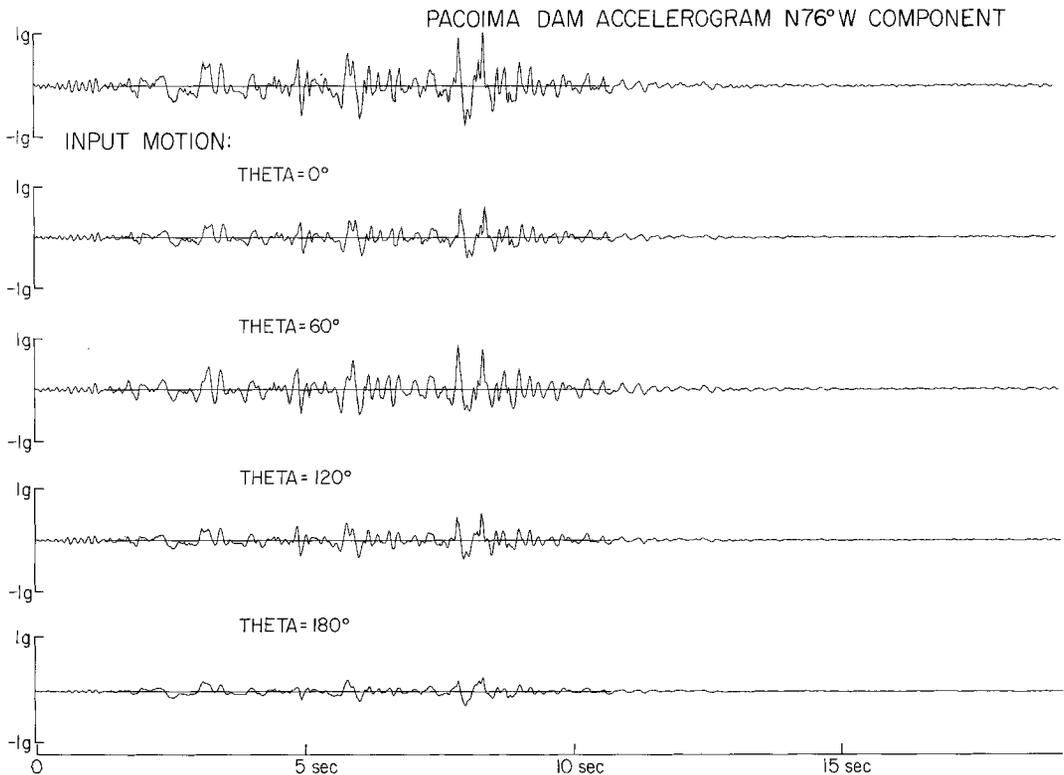
FIG. 6. Amplitudes of incoming SH waves for selected angles of incidence.

of incidence. For high frequencies, large differences in amplitudes occur for $\theta = 0°$ and $\theta = 180°$ because nearly direct reflection of incident waves causes the front side of the canyon to have higher amplitudes than the sheltered far side. For the nearly vertically incident waves, ($\theta = 60°$ and $\theta = 120°$), the moduli of the transfer functions are more nearly uniform and deviate about ± 50 per cent from the value of 2 for the featureless half-space.

The transfer functions, $T_{0j}(\omega)$ for points on the profiles of the example canyon may be used to make a calculation illustrating the potential effects of canyon topography upon strong ground motions. The transient motion used in the analysis is the N76°W component of the accelerogram recorded at Pacoima Dam in the 1971 earthquake. It is
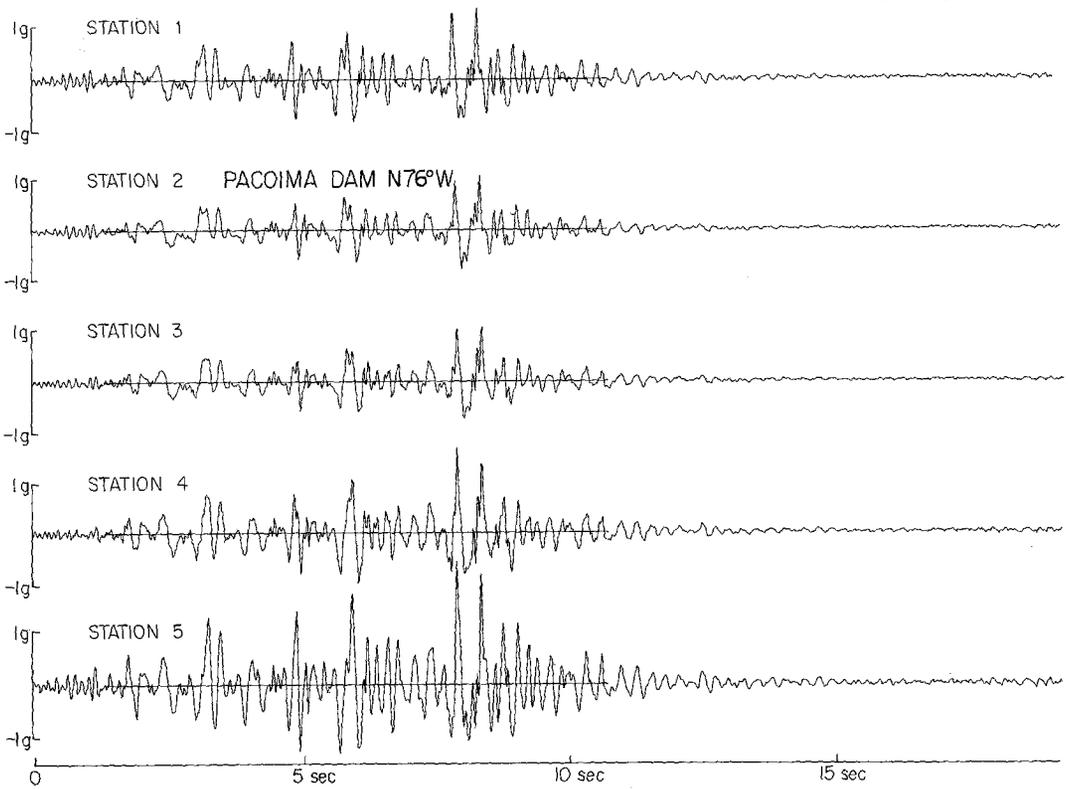
THETA = 60°

STATION 1

STATION 2   PACOIMA DAM N76°W

STATION 3

STATION 4

STATION 5

0   5 sec   10 sec   15 sec

FIG. 7. Calculated accelerations at stations in cross-section C for *SH* waves with angle of incidence, $\theta = 60°$.

THETA = 120°

STATION 1

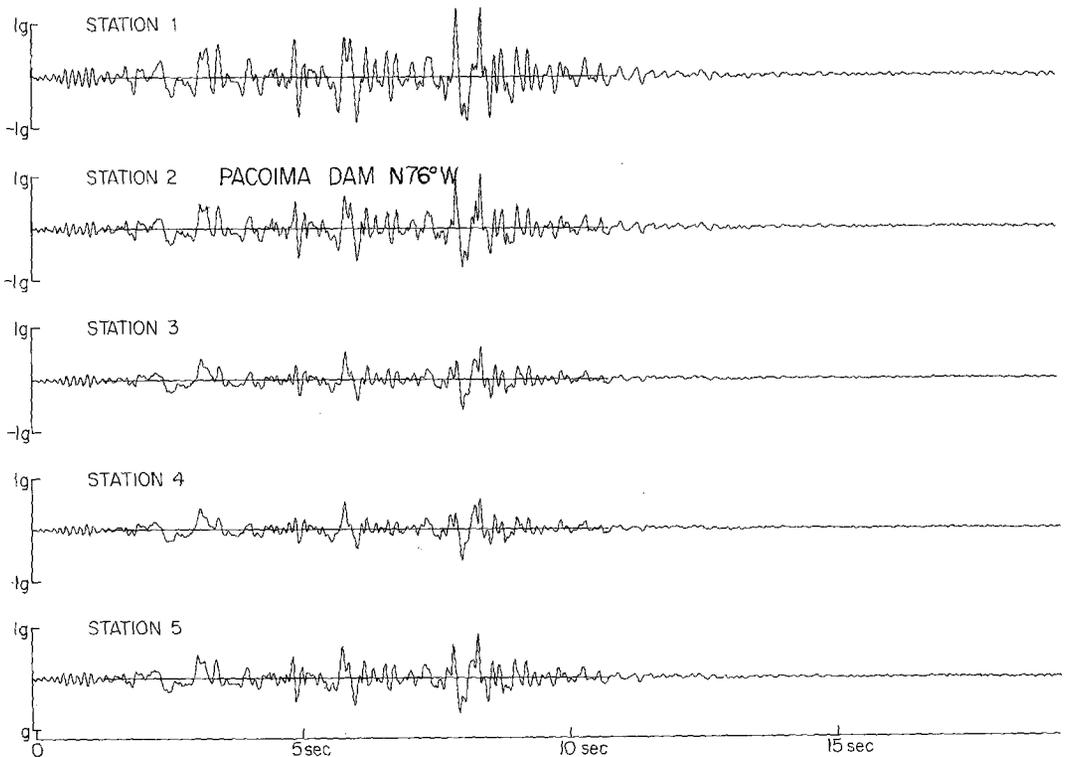STATION 2   PACOIMA DAM N76°W

STATION 3

STATION 4

STATION 5

0   5 sec   10 sec   15 sec

FIG. 8. Calculated accelerations at stations in cross-section C for *SH* waves with angle of incidence, $\theta = 120°$.

assumed in the analysis that this record represents the *SH* motion observed at the surface at point 2 and that the incoming motion to the canyon is planar, with a constant angle of incidence.

With the motion specified at point 2, the unknown incident motion becomes a function of the angle of incidence. The transfer functions $T_{0j}(\omega)$ were used to compute the incident motion required to produce the given motion at point 2 for four angles of incidence. These results are given in Figure 6 along with the acceleration specified to occur at point 2. The smallest incident wave is required for $\theta = 180°$ because of focusing effects noted previously. It should be recalled when comparing the motions in Figure 6 that if the *SH*-waves were incident on a flat surface, the incident motion would be half the specified surface motion, and the motion within the half-space would be a superposition of the incident and reflected waves.

Accelerograms at other locations were next calculated from the inputs associated with different angles of incidence. Results for 60° and 120° are plotted in Figures 7 and 8, respectively. The motion at point 2 is also included in those figures for purposes of comparison. Although the accelerograms are similar in form, there are obvious differences in peak values and general levels of motion. There is a strong effect resulting from the angle of incidence; for example, the motion at station 4 appears stronger than at station 2 for $\theta = 60°$ and weaker than at 2 for $\theta = 120°$. The exterior stations 1 and 5 tend to show the largest response while the interior stations 2, 3 and 4, tend to be of more nearly the same level. Because of the limitations of the assumptions, the analysis cannot be considered to be a precise description of the real earthquake motions, particularly for higher frequencies, but it is thought that the results do indicate the type of effects that might occur under similar but more complicated conditions.

In earthquake engineering practice, the significance of potential differences in the motion are usually judged by examination of response spectra, rather than accelerograms or transfer functions. Response spectra portray the maximum values of the response of simple, one degree-of-freedom structures of varying periods and dampings to the given accelerogram, and are of fundamental importance in earthquake engineering (Housner, 1959, Neumark and Rosenblueth, 1971). Response spectra for 5-per cent damping were calculated from accelerograms selected from those shown in Figures 7 and 8. The spectra, including those which appeared to be most different, are given in Figures 9 and 10. Figure 9 shows the individual spectra, while Figure 10 portrays three of the curves on the same plot, indicating the maximum variation among the spectra. It is seen in the plots that the larger differences are confined to periods less than 1 sec. The spectra for the interior points 2, 3 and 4 are of about the same level, while the largest spectrum comes from the accelerogram at station 5 for an angle of incidence of 60°, which is consistent with the appearance of the accelerogram which is clearly larger than the others (Figure 7). It is again noted that station 5 and station 1, which both show relatively strong amplification, are located at the 90° corners joining the profile and the flat surface.

Pacoima Dam lies about 5 miles south of the epicenter of the San Fernando earthquake and about the same distance north of the zone where fault rupture was observed on the surface of the ground (Trifunac and Hudson, 1971). The hypocentral depth of the earthquake was in the range from 6 to 8 miles. This geometry indicates that of the two angles of incidence used in the calculations, 60° would be most appropriate for waves emanating from the epicentral area, whereas 120° would most closely approximate the motion originating from that portion of the fault nearer the ground surface, which ruptured later in time than the epicentral zone. These two portions are thought to have shown the greatest relative movements during the earthquake (Trifunac, 1974). It is seen from Figures 7 and 8 that a change in the angle of incidence from 60° to 120° at some time in
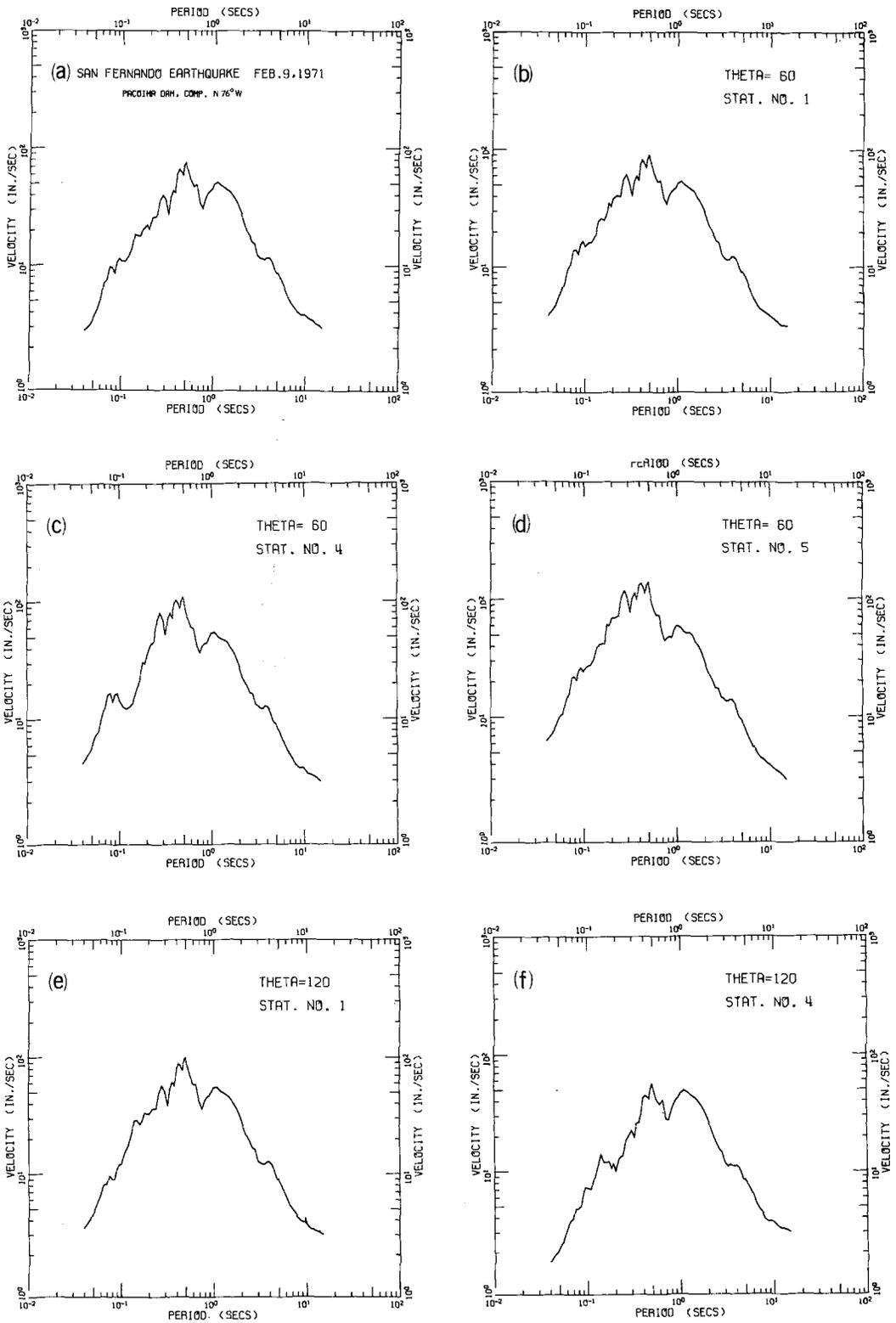
FIG. 9. Response spectra of the Pacoima Dam accelerogram and selected accelerograms from Figures 7 and 8.

the first few seconds of motion would tend to reduce the level of amplification of motion at stations 3, 4, and 5 over that at station 2. It seems fair to infer from this comparison that the real situation with waves originating from several angles of incidence would also tend to have an averaging effect on the level of motion.

DISCUSSION

The calculation method presented herein has several advantages for application to problems in earthquake engineering and seismology. The ability to treat realistic, two-dimensional topography, to consider waves of arbitrary incidence, and to study transient motions is illustrated by the example calculations. In addition, it is noted that the
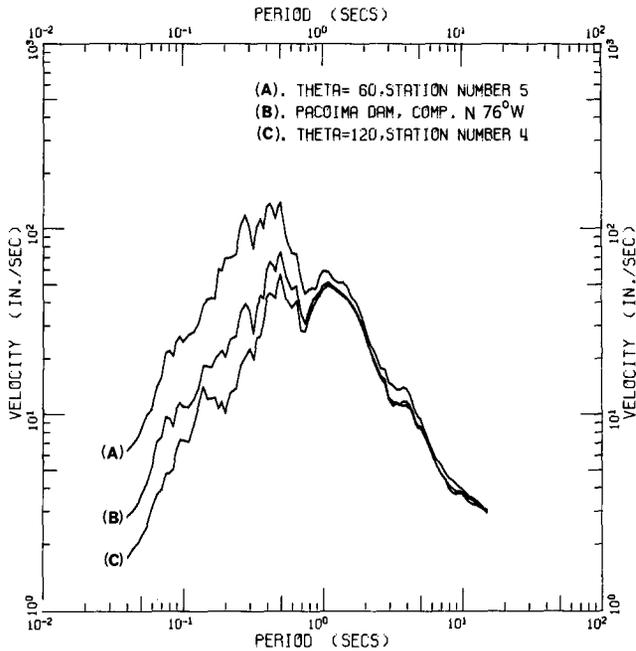

FIG. 10. Comparison of three response spectra from Figure 9. Spectra A is from a station where the motion is strongly amplified; B is the spectra from the Pacoima Dam record; and C is from a shielded area.

approach is convenient for examining problems involving low frequencies, because the number of grid points can be relatively small. The method can easily handle discontinuities in the material properties, provided their number is not large, because only values at the boundaries have to be considered, rather than values at points in the media as is required by methods using finite elements or finite differences.

The example calculations utilized harmonic displacement amplitudes, transfer functions, accelerograms, and response spectra to investigate the degree of similarity or difference that might be expected in strong ground motion because of effects of canyon-type topography. It is clear from the figures that these different measures highlight different features of the problem and that they give different impressions of the amount and significance of observed differences. In this regard the harmonic displacement amplitudes and transfer functions indicate larger differences than are seen on the accelerograms, at least in this example, and the response spectra show the smallest differences.

Which measure is the most appropriate depends to some extent on the application in question. From the point of view of selecting criteria for earthquake-resistant design, where the decision is often reduced to the determination of the amplitude of a smooth design spectrum of standard shape, it seems most appropriate to examine differences in the response spectra. That is to say, differences in the motion too small to show up on the response spectra are not significant enough to affect the choice of design criteria.

The analysis presented assumes two-dimensional motion, simplified wave motions, and homogeneous elastic material, and it is difficult to assess the applicability of such analyses to the much more complicated situations that arise in actuality. Unfortunately, there are not yet enough strong-motion data to guide this assessment effectively and the matter is primarily one of individual judgment. It is the authors' opinion that analyses such as presented above can indicate the frequency band over which topographic effects are not likely to be important and give indications of the nature and amplitudes of topographic effects for low frequencies. For higher frequencies, the analysis only serves as a qualitative guide to the differences that might be expected.

One potential application of the analysis is in the calculation of the earthquake response of large structures, such as suspension bridges, where one of the important questions is the correlation and phasing of the earthquake excitation at different parts of the structural foundations, which are often separated by canyon topography. For various types of assumed wave motion, the method could be used to estimate the shaking at points of interest.

REFERENCES

Adams, W. M., E. K. Schubel, and E. Schlesinger (1964). Wave propagation phenomena at an irregular infinite interface, Part II: Free surface case, *Bull. Seism. Soc. Am.* **54**, 2223–2232.

Aki, K. and K. L. Larner (1970). Surface motion of a layered medium having an irregular interface due to incident plane *SH* waves, *J. Geophys. Res.* **75**, 933–954.

Asano, S. (1966). Reflection and refraction of elastic waves at a corrugated surface, *Bull. Seism. Soc. Am.* **56**, 0201–0222.

Banaugh, R. P. and W. Goldsmith (1963a). Diffraction of steady elastic waves by surfaces of arbitrary shape, *J. Appl. Mech.* **12**, 589–597.

Banaugh, R. P. and W. Goldsmith (1963b). Diffraction of steady acoustic waves by surfaces of arbitrary shape, *J. Acoust. Soc. Am.* **35**, 1590–1601.

Banaugh, R. P. (1965). Remarks on a series of three papers, "Wave Propagation Phenomena at an Irregular Infinite Interface: Part I, II, III", by W. H. Adams *et al.*, *Bull. Seism. Soc. Am.* **55**, 1053–1058.

Boore, D. M. (1972). A note on the effect of simple topography on seismic *SH*-waves, *Bull. Seism. Soc. Am.* **62**, 0275–0284.

Boore, D. M. (1973). The effect of simple topography on seismic waves: Implications for the accelerations recorded at Pacoima Dam, San Fernando Valley, California, *Bull. Seism. Soc. Am.* **63**, 1603–1609.

Bouchon, M. (1973). Effect of topography on surface motion, *Bull. Seism. Soc. Am.* **63**, 715–632.

de Hoog, F. and R. K. Weiss (1973). On the solution of a Volterra integral equation with a weakly singular kernel, *SIAM, J. Numerical Anal.* **10**, 647–665.

Housner, G. W. (1959). Behavior of structures during earthquakes, *J. Eng. Mech. Div.*, ASCE **85**, 109–130.

McIvor, I. K. (1969). Two-dimensional scattering of plane compressional wave by surface imperfections, *Bull. Seism. Soc. Am.* **59**, 1359–1364.

Morse, P. M. and H. Feshbach (1953). *Methods of Theoretical Physics*, McGraw-Hill, New York.

Mow, C. C. and Y. H. Pao (1971). The Diffraction of Elastic Waves and Dynamic Stress Concentrations, *RAND Report, R-482-PR*.

Newmark, N. M. and E. Rosenblueth (1971). *Fundamentals of Earthquake Engineering*, Prentice-Hall, Englewood Cliffs, New Jersey.

Reimer, R. B., R. W. Clough, and J. M. Raphael (1974). Seismic response of Pacoima Dam in the San Fernando Earthquake, *Proc. World Conf. Earthquake Eng., 5th, Rome* **2**, 2328–2337.

Shafai, L. (1970). An improved integral equation for the numerical solution of two dimensional diffraction problems, *Can. J. Physics* **48**, 954–963.

Sharma, D. L. (1967). Scattering of steady waves by surfaces of arbitrary shape, *Bull. Seism. Soc. Am.* **57**, 0795–0812.

Trifunac, M. D. and D. E. Hudson (1971). Analysis of the Pacoima Dam accelerogram—San Fernando, California, earthquake of 1971, *Bull. Seism. Soc. Am.* **61**, 1393–1411.

Trifunac, M. D. (1973). Scattering of plane *SH*-waves by a semi-cylindrical canyon, *Intern. J. Earthquake Eng. and Stress Dynamics* **1**, 267–281.

Trifunac, M. D. (1974). Three-dimensional dislocation model for the San Fernando, California, earthquake of February 9, 1971, *Bull. Seism. Soc. Am.* **64**, 149–172.

Wong, H. L. and M. D. Trifunac (1974). Scattering of plane *SH*-waves by a semi-elliptical canyon, *Intern. J. Earthquake Eng. and Stress Dynamics* **3**, 157–169.

EARTHQUAKE ENGINEERING RESEARCH LABORATORY
CALIFORNIA INSTITUTE OF TECHNOLOGY
PASADENA, CALIFORNIA 91125